The Journal of Experimental Biology 209, 4452-4463
Published by The Company of Biologists 2006
doi:10.1242/jeb.02537

Interaction of two swimming *Paramecia*

Takuji Ishikawa[1,*] and Masateru Hota[2]

[1]*Department of Bioengineering and Robotics, Graduate School of Engineering, Tohoku University, Aoba 6-6-01, Sendai 980-8579, Japan and* [2]*Department of Mechanical Engineering, University of Fukui, 3-9-1 Bunkyo, Fukui 610-8507, Japan*

*Author for correspondence (e-mail: ishikawa@pfsl.mech.tohoku.ac.jp)

Accepted 8 September 2006

Summary

The interaction between two swimming *Paramecium caudatum* was investigated experimentally. Cell motion was restricted between flat plates, and avoiding and escape reactions were observed, as well as hydrodynamic interactions. The results showed that changes in direction between two swimming cells were induced mainly by hydrodynamic forces and that the biological reaction was a minor factor. Numerical simulations were also performed using a boundary element method. *P. caudatum* was modelled as a rigid spheroid with surface tangential velocity measured by a particle image velocimetry (PIV) technique. Hydrodynamic interactions observed in the experiment agreed well with the numerical simulations, so we can conclude that the present cell model is appropriate for describing the motion of *P. caudatum*.

Key words: hydrodynamic interaction, *Paramecium caudatum*, biological reaction, swimming motion, numerical simulation.

Introduction

It is important to understand and predict the flow of suspensions of micro-organisms that appear in massive plankton blooms in the ocean, harmful red tides in coastal regions and are used in bioreactors. The size of individual micro-organisms is often much smaller than that of the flow field of interest, so the suspension is modelled as a continuum in which the variables are volume-averaged quantities (Fasham et al., 1990; Pedley and Kessler, 1992; Metcalfe et al., 2004). Continuum models for suspensions of swimming micro-organisms have also been proposed for the analysis of phenomena such as bioconvection (e.g. Childress et al., 1975; Pedley and Kessler, 1990; Hillesdon et al., 1995; Bees and Hill, 1998; Metcalfe and Pedley, 2001). However, the continuum models proposed so far are restricted to dilute suspensions, in which cell–cell interactions are negligible. If one wishes to consider larger cell concentrations, it will be necessary to consider the interactions between micro-organisms. Then, the translational–rotational velocity of the micro-organisms, the particle stress tensor and the diffusion tensor in the continuum model will need to be refined.

To understand the interactions between micro-organisms, it is first necessary to clarify two-cell interactions. Thus, we investigated the interaction between two model micro-organisms analytically (Ishikawa et al., 2006), assuming that the cell–cell interaction is purely hydrodynamic; no biological reactions were considered. In practice, however, it is to be expected that in the presence of a nearby micro-organism, a given micro-organism would not behave as if it were alone. A micro-organism may consider reproducing sexually or attempting to consume (or avoid being consumed by) its neighbour. It may also move away from it, because of the increased competition for food. Although two-cell interactions are important when considering the interactions between many cells, it is not at all clear how cells behave when they are in close contact. Also, cell–cell interactions were not modelled precisely in any previous analytical studies dealing with a non-dilute suspension of micro-organisms (Guell et al., 1988; Ramia et al., 1993; Nasseri and Phan-Thien, 1997; Lega and Passot, 2003; Jiang et al., 2002). In this study, we clarify how two micro-organisms interact when they come close to each other, both experimentally and numerically.

Paramecium caudatum was used in this study, because the behavior of individual cells of this organism is well understood. Naitoh and Sugino investigated two types of biological reactions of a solitary *Paramecium* cell to mechanical stimulations (Naitoh and Sugino, 1984). (i) Avoiding reactions occur when a cell bumps against a solid object with its anterior end. The cell swims backward first, gyrates about its posterior end, and then resumes normal forward locomotion. (ii) Escape reactions occur when the cell's posterior end is mechanically agitated. The cell increases its forward swimming velocity for a moment, then resumes normal forward locomotion. The change in the swimming motion is regulated by changes in membrane potential, because *Paramecium* cells, like other monads, have no nerves for transmitting stimulative information nor synapses to determine transmission direction. Machemer clarified the frequency and directional responses of

cilia to changes in membrane potential in *Paramecium* cells (Machemer, 1974). There are many Ca^{2+} channels in the anterior end, whereas there are many K^+ channels in the posterior end. The locality of the ion channels is the essential mechanism controlling *Paramecium*'s biological reaction (Naitoh and Sugino, 1984). In reality, the range of micro-organism lengths is large, and they alter their behaviour according to many environmental parameters. The variety of shapes both within and between species is also vast (Brennen and Winet, 1977). Many types of ciliate, however, show a similar biological reaction to that of *Paramecium* cells, because they also have Ca^{2+} channels in the anterior end and K^+ channels in the posterior end. We focused on *Paramecium* cells in the present study, but we expect that our results will be applicable to other ciliates and micro-organisms.

The interaction between two *P. caudatum* cells was investigated both experimentally and numerically. Cell motion was restricted between flat plates with a gap of about 70 μm. We observed avoiding and escape reactions as well as hydrodynamic interactions. To conclude that the interaction is purely hydrodynamic, it is necessary to simulate the cells' motion numerically without any biological response. Thus, the *P. caudatum* cell was modelled as a rigid spheroid with prescribed surface tangential velocities measured by a particle image velocimetry (PIV) technique. The model is referred to as a 'squirmer', and is explained briefly in Materials and methods (for details, see Ishikawa et al., 2006). The interaction between two squirmers was calculated by a boundary element method, and the results were compared with those of the experiments. The authors have used a squirmer model for other studies (Ishikawa et al., 2006; Pedley and Ishikawa, 2004) (J. Ishikawa and T. J. Pedley, manuscript submitted for publication), so a comparison was also made with the earlier data to check the reliability of the squirmer model.

Materials and methods

Materials and experimental setup

Cultures of the unicellular freshwater ciliate *Paramecium caudatum* Ehrenberg were used for the experiments. They were grown by inoculating 2 ml of a logarithmic-phase culture into 250 ml of culture fluid. The culture fluid was made by boiling demineralised water with 2 g of straw, then adding 0.2 g of yeast powder. It was kept at 20°C for 2 weeks before inoculation. Measurements were performed 2 weeks after inoculation of the culture at 19–21°C. Microscopic observation showed that the body length of an individual cell was in the range of approximately 200–250 μm and the width approximately 40–50 μm. The swimming speed of an individual cell was approximately 1 mm s^{-1}. The swimming motion of *P. caudatum* in a free space is not straight, but forms a left spiral. The pitch of the spiral was approximately 2 mm and the width was 0.4 mm.

The experimental setup was designed to measure the displacements of cells in a still fluid between flat plates (Fig. 1). The motion of cells was restricted to two-dimensions for the following two reasons: (i) the orientation vector of the cell and the distance between two surfaces of cells were easy to measure without a considerable error, and (ii) biological reactions were observed much more frequently in two-dimensional space, because cells experienced strong collisions when there was no height variation. The latter reason is important in order to analyse a large number of biological reactions. The experimental setup consisted of a digital video (DV) camera with a 24× macrolens, light sources, and inner and outer dishes. The test fluid was placed between the top of the outer dish and the bottom of the inner dish. The gap between the two dishes was about 70 μm, so that cells could not overlap three-dimensionally. The test fluid was same as the culture fluid, but the volume fraction of cells was adjusted to within about 0.5–1% so that three-cell interactions rarely occurred. Cell movements were recorded by the DV camera over a 10–20 min period, and we did not observe any decrease in the cells' swimming velocity or aggregation due to the cell chemotaxis during the measurements.

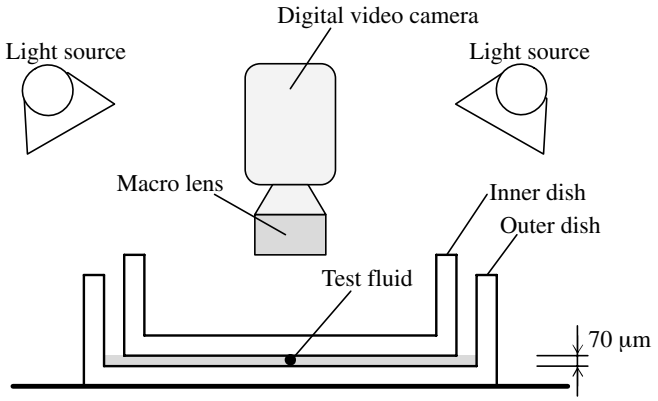

Fig. 1. Schematics of the experimental apparatus. Test fluid was placed between the bottom of the inner dish and the top of the outer dish.

Sample sequences of the interaction between two swimming *P. caudatum* observed in the experiment are shown in Fig. 2. The time interval for each sequence is Δt=1/3s, and the background is subtracted from the figure by image processing. We observed such interactions several times per 10–20 min experiment. Since the intention was to concentrate on two-cell interactions, data were deleted if there was a third cell within 750 μm of one of the two interacting cells. The velocity disturbance caused by a force-free cell near a wall boundary decays as r^{-2}, where r is the distance from the cell, so the effect of the third cell on the swimming velocities of the two interacting cells is less than about 10% if it is farther than 750 μm away. (The derivation of velocity disturbance due to a force-free particle near a wall boundary is shown in Appendix A.) Microscopic observation showed that some solitary cells occasionally stopped swimming, even though there seemed to be no mechanical stimulation. They then swam backward, gyrated about their posterior ends, and finally resumed normal forward locomotion. Such a reaction is rare if one uses a culture

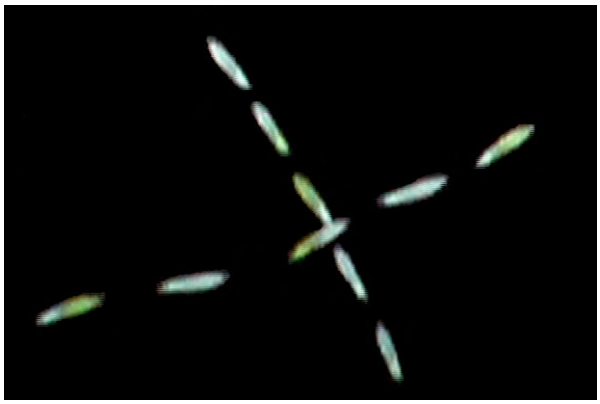

Fig. 2. Sequences showing the interaction of two swimming *P. caudatum* cells observed in the experiment. The background was subtracted from the figure.

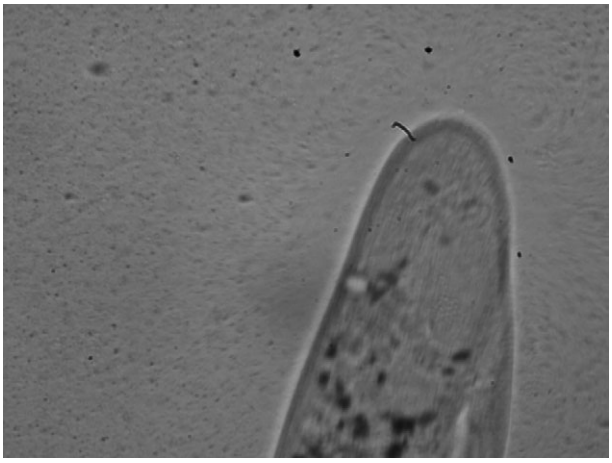

Fig. 3. Original image for a swimming *P. caudatum* cell in a water with a small amount of milk between flat plates.

2 weeks after the inoculation, but could not be eliminated completely. Since we intended to measure two-cell interactions, data were deleted if one of two interacting cells showed this type of solitary reaction before the two cells approached within a distance of L, where L is the body length of the shorter cell. The interaction data was recorded regardless of whether it was a biological reaction or a hydrodynamic interaction, and the total number of data recorded in this study was 301.

Surface velocity of P. caudatum

The velocity field around a swimming *P. caudatum* cell between flat plates was measured using a PIV technique. A small amount of milk was added to the culture fluid as tracer particles, and the flow field was recorded using a CMOS camera (Basler A602f; 659×493 pixels, 100 frames s^{-1}; Basler AG, Ahrensburg, Germany) through a microscope. A sample original image is shown in Fig. 3. The velocity vector was calculated from two successive images using a MatPIV (Grue et al., 1999), in which spurious vectors were removed by a signal-to-noise ratio filter (cf. Keane and Adrian, 1992), a global histogram operator and a median filter. The spurious vectors were replaced by vectors linearly interpolated from neighbouring points. The velocity vector was calculated for a time series of images, and approximately 80 000 velocity vectors around a swimming cell were obtained. These vectors were averaged by assuming that the velocity field is axisymmetric and time-independent. The velocity field relative to the cell's swimming velocity vector is shown in Fig. 4. We see that the cell swims smoothly without generating a recirculation region.

The surface velocity of *P. caudatum* has to be measured for use as a boundary condition for the numerical simulation, as explained in below. We intended to measure the surface velocity of the cell by the PIV technique; however, the method showed considerable instability at short wavelengths, so we could not accurately measure the velocity vector using this method. Thus, we interpolated surface velocity as follows. A cell was assumed to be an extended ellipsoid with a minor axis of 0.36, where length was nondimensionalised relative to the major axis. The surface velocity vectors were interpolated linearly from those at 0.18 and 0.36 from the surface with the same angle θ from the orientation vector of the cell. We assumed that surface velocity was mainly tangential, because

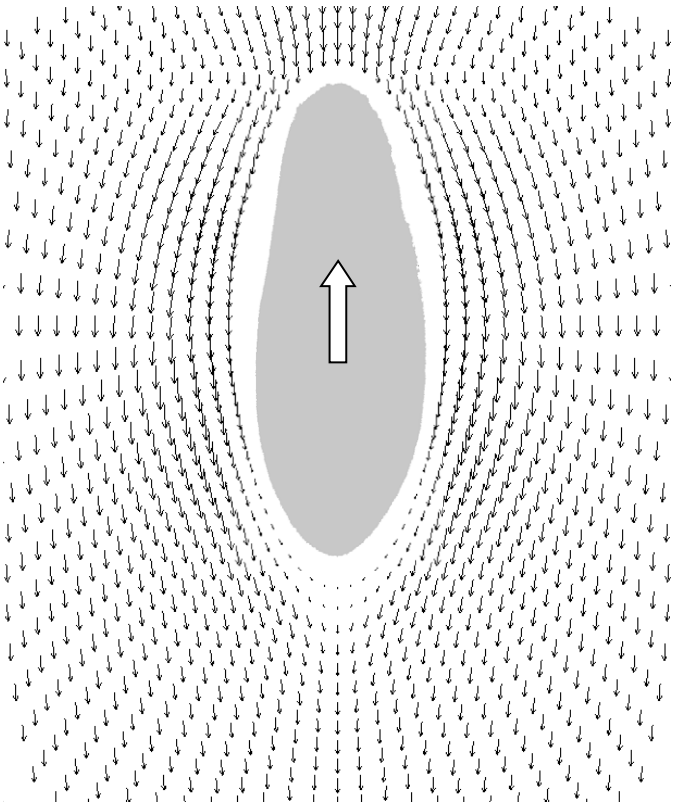

Fig. 4. Velocity vectors relative to the swimming velocity of *P. caudatum*, which were calculated by the PIV methods by assuming that the velocity field is axisymmetric and time-independent. The large arrow indicates the swimming direction of the cell.

cells did not deform and fluid did not penetrate its surface at high velocities. The tangential surface velocity, u_s, interpolated from the PIV data is shown in Fig. 5. We see that u_s is faster near the anterior end than near the posterior end.

The experimental results of u_s were approximated by:

$$u_s \approx \sum_{i=1}^{5} c_i \sin(i\theta) , \quad 0 \leqslant \theta \leqslant \pi , \tag{1}$$

where coefficients c_i were determined by the method of least squares (c_1=1.707, c_2=0.2400, c_3=0.2472, c_4=0.1506, c_5=0.1154). u_s (Eqn 1) is also shown in Fig. 5. The high modes decay faster than the low modes as the distance from the cell increases; thus, the far-field velocity is governed by the lowest mode (cf. Ishikawa et al., 2006). Moreover, the role of high modes in the near-field is to generate fluctuations in velocity. Hence, the overall properties, such as the trajectories of a pair of cells, may be captured by the first few modes. Thus, we used up to the fifth mode in Eqn 1, which was used as a boundary condition for the cell surface (cf. *Numerical methods*, below).

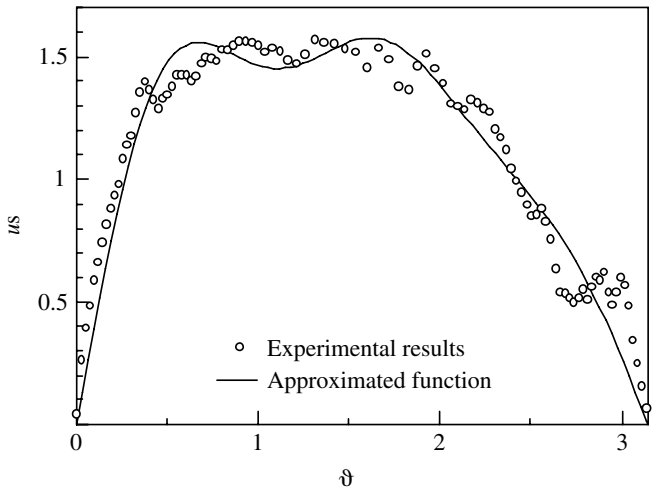

Fig. 5. Experimental results and an approximated curve defined by Eqn 1 for a surface velocity of *P. caudatum*. The coefficients in Eqn 1 are c_1=1.707, c_2=0.2400, c_3=0.2472, c_4=0.1506 and c_5=0.1154.

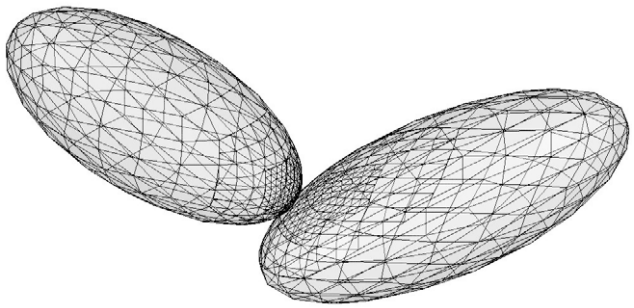

Fig. 6. Computational mesh for two interacting squirmers, in which 590 triangle elements are generated per squirmer. The mesh is finer in the near-contact region. Using the boundary element method, the computational mesh is generated only on the particle surfaces.

Numerical methods

The *P. caudatum* cell was modelled as a rigid spheroid with the surface tangential velocity measured by the PIV technique, referred to as a 'squirmer'. The squirmer model was first proposed by Lighthill (Lighthill, 1952), and his analysis was then extended (Blake, 1971a). The numerical methods used in this study are similar to those reported elsewhere (Ishikawa et al., 2006), so only a brief explanation is given here. A squirmer is assumed to be neutrally buoyant and torque-free. The Reynolds number based on the swimming speed and the radius of individuals is small, so that the flow field can be assumed to be a Stokes flow. Brownian motion is not taken into account, because a cell is too large for Brownian effects to be important. The spheroid's surface is assumed to move purely tangentially and this tangential motion is assumed to be axisymmetric and time-independent. The tangential surface velocity of a squirmer is given by Eqn 1. We performed a trial simulation for a solitary squirmer swimming in a still fluid with the boundary condition of Eqn 1. The results showed that the swimming velocity of the squirmer was 1.04, although it should be 1.0 because the

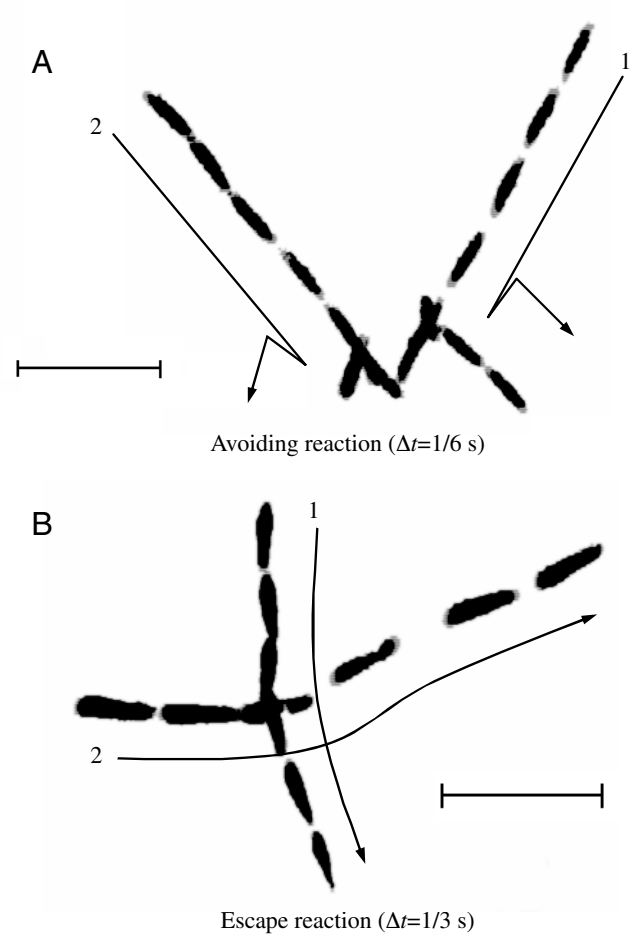

Fig. 7. Sequences showing the biological reactions when two swimming *P. caudatum* (labeled 1, 2) experience a near-contact. Long arrows are added to schematically show cell motion. (A) Avoiding reaction (Δt=1/6 s). (B) Escape reaction (Δt=1/3 s). Scale bars, 500 μm.

surface velocity is non-dimensionalized by the swimming velocity. The error may arise from the u_s approximation, although it is very small.

When there are two squirmers in an infinite fluid otherwise at rest, the Stokes flow field external to the squirmers can be given in an integral form as:

$$\mathbf{u}(\mathbf{x}) = -\sum_{m=1}^{2} \int_{A'_m} \mathbf{K}(\mathbf{x}-\mathbf{x}') \cdot \mathbf{q}(\mathbf{x}')\mathrm{d}A'_m , \qquad (2)$$

where A_m is the surface of squirmer m and $\mathbf{K}$ is the Oseen tensor. The single-layer potential, $\mathbf{q}$, is the subtraction of the traction force on the inner surface from that on the outer surface. The boundary condition is given by:

$$\mathbf{u}(\mathbf{x}) = \mathbf{U_m} + \boldsymbol{\Omega}_\mathbf{m} \wedge (\mathbf{x}-\mathbf{x_m}) + \mathbf{u_{s,m}} , \qquad \mathbf{x} \in A_m , \qquad (3)$$

where $\mathbf{U_m}$ and $\boldsymbol{\Omega}_\mathbf{m}$ are the translational and rotational velocities of squirmer m, respectively. $\mathbf{x_m}$ is the centre of squirmer m, and $\mathbf{u_{s,m}}$ is the squirming velocity of squirmer m, given by Eqn 1. In simulating hydrodynamic interactions between two squirmers, we assume that the surface velocity is independent of the distance between the cells. Thus, no biological reaction is modelled, and the interaction is purely hydrodynamic. Similarly to Ishikawa et al. (Ishikawa et al., 2006), we employed another boundary condition of constant swimming power; however, the difference in trajectories was very small (see Appendix B).

In the experiment, two cells swim between flat plates, and the motion of cells was restricted to a two-dimensional plane. In the numerical simulation, on the other hand, squirmers swim in an infinite fluid, but the centres and orientation vectors of two squirmers were initially set in the same plane. The motion of squirmers remained in the plane, even though the flow field is three-dimensional, because the surface squirming velocity is axisymmetric. The two flat plates were omitted in the simulation, because adding them does not qualitatively affect the interaction provided that the two squirmers remain in the same plane. The quantitative effect of wall boundaries on the swimming speed was also small (see Appendix C).

The boundary element method was employed to discretize Eqn 2. The computational mesh used in this study is shown in Fig. 6. A maximum of 590 triangle elements per particle were generated, and the mesh was finer in the near-contact region. Time-marching was performed by 4th-order Runge–Kutta schemes. A non-hydrodynamic interparticle repulsive force, $\mathbf{F_{rep}}$, was added to the system in order to avoid the prohibitively small time step needed to overcome the problem of overlapping particles. We followed published methods (Brady and Bossis,

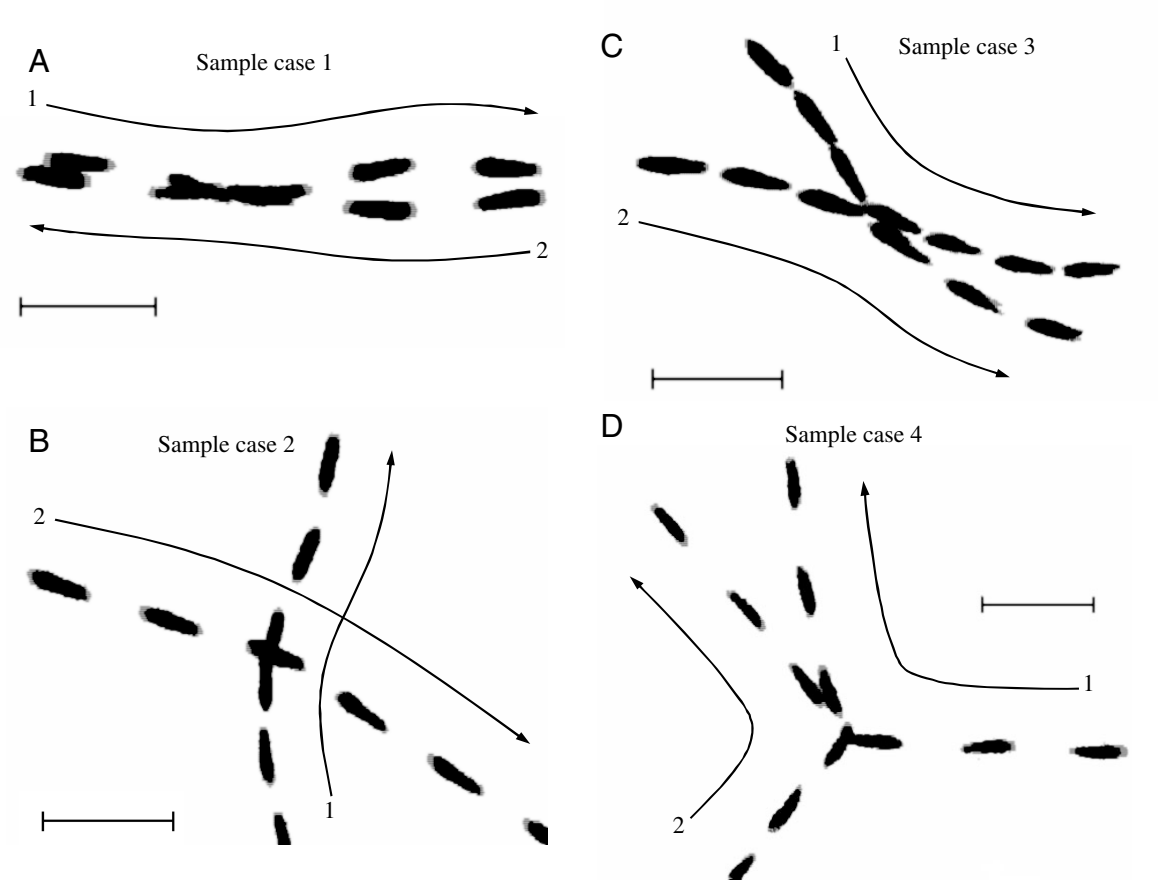

Fig. 8. Some sample sequences showing the hydrodynamical interactions when two swimming *P. caudatum* experience a near-contact. The time interval between each sequence is 1/3 s. Long arrows are added to schematically show cell motion. (A) Sample case 1; (B) sample case 2; (C) sample case 3; (D) sample case 4. Scale bars, 500 μm.

Table 1. *Ratio of three types of interaction*

Type of interaction	Number of cells	Percentage (%)
Hydrodynamic interaction (HI)	510	84.7
Avoiding reaction (AR)	29	4.8
Escape reaction (ER)	63	10.5

Total number of experimental cases recorded in this study, 301; total number of cells, 602.

1985) (T. Ishikawa and T. J. Pedley, manuscript submitted for publication), and used the following function:

$$\mathbf{F}_{\mathbf{rep}} = \alpha_1 \frac{\alpha_2 \exp(-\alpha_2 \epsilon)}{1 - \exp(-\alpha_2 \epsilon)} \frac{\mathbf{h}}{h}, \quad (4)$$

where α_1 is a dimensional coefficient, and α_2 is a dimensionless coefficient. ϵ is the minimum separation between two surfaces, which was calculated by the iterative methods proposed (Claeys and Brady, 1993). The separation vector **h** connects the minimum separation points on the two surfaces. The coefficients used in this study were α_1=0.1 and α_2=10^3. The minimum separation obtained using these parameters was in the range 10^{-3}–10^{-4}. The effect of the repulsive force on the trajectories of cells was very small, because it acts only in the very near field and changes the distance between particles by only approximately 10^{-4}. This was confirmed numerically by comparing three trajectories, which are shown in Figs 9–11, with and without a repulsive force.

Results

Experimental results

Before analysing the results of two-cell interactions, we show some typical observation results in order to help readers understand the phenomena. Fig. 7A shows an avoiding reaction, in which arrows are drawn to schematically show cell motion. The time interval for each sequence is Δt=1/6s and the colour is reversed from the original figure (as shown in Fig. 2). We see that two cells collide with their anterior ends. They first swim backward, then gyrate about their posterior ends, then resume normal forward locomotion. We defined an avoiding reaction as one involving backward swimming during the interaction.

Fig. 7B shows an escape reaction, which occurs when the cell's posterior end is strongly agitated. We see that cell 2 increases its forward swimming velocity after the collision. The original movie was taken 30 frames s^{-1}, and the velocity vector of a cell was calculated by tracking the centre of the major axis of the cell in each frame. If a cell's swimming velocity after the collision became 1.3 times faster than the initial value, we classified the interaction as an escape reaction, where the initial value was defined when two cells' surfaces were at a distance of *L* before the collision.

When a cell–cell interaction did not satisfy the definition of an avoiding reaction (AR) nor that of an escape reaction (ER), it was classified as a hydrodynamic interaction (HI). Four kinds of typical HI results are shown in Fig. 8. When two cells are initially facing, they come close to each other at first, then they change their directions slightly in the near field, and finally move away from

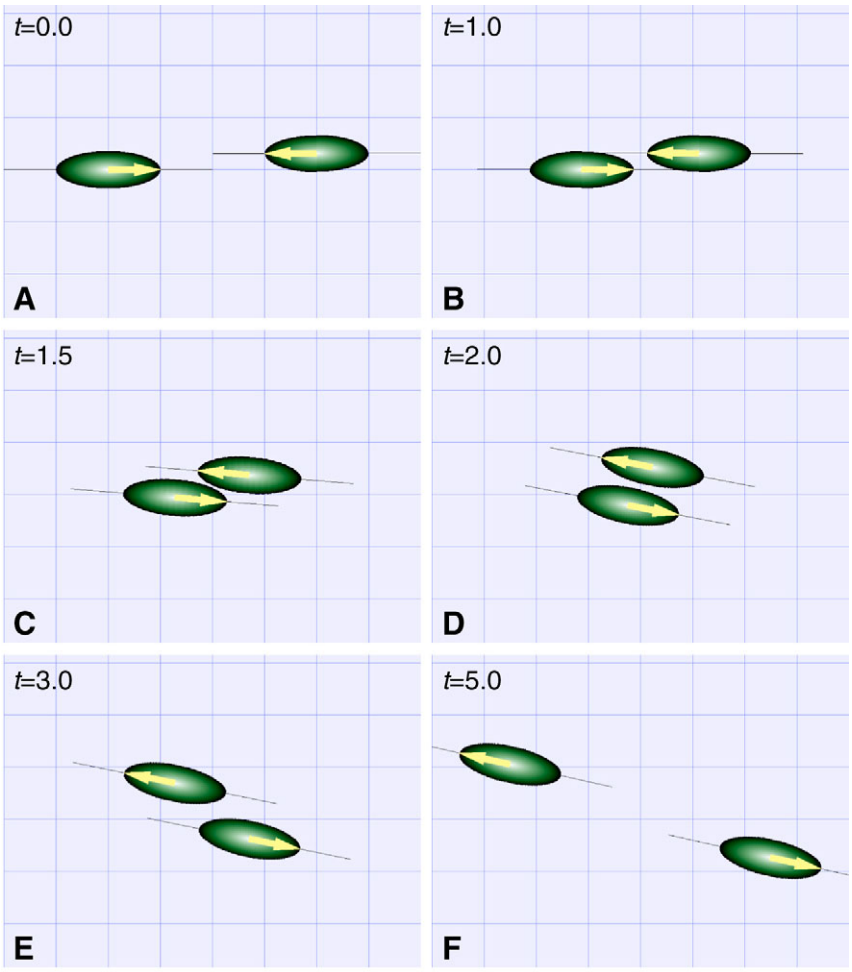

Fig. 9. Sequences (A–F) showing the hydrodynamic interactions between two squirmers under the initial condition of $\theta_{in} \approx \pi$. At *t*=0, there is a distance of 0.3 in the perpendicular direction to the orientation vectors, where *t* is the dimensionless time and *t*=0 is the initial instant. The orientation vectors of the squirmers are shown as large arrows on the ellipsoids, and a thin solid line is added so that one can easily compare the angle between the two squirmers. $d\theta$, explained in Fig. 12, is about 0.0 in this case. (A) *t*=0.0; (B) *t*=1.0; (C) *t*=1.5; (D) *t*=2.0; (E) *t*=3.0; (F) *t*=5.0.

each other (see Fig. 8A). The change in direction is small in this case. When the initial angle between the orientation vectors of the two cells is less than about $3\pi/4$, there are two main kinds of swimming motions. If one cell collides with the posterior end of the other cell, the two cells do not significantly change their swimming direction, as shown in Fig. 8B. On the other hand, if one cell collides with the anterior end of the other cell, the two cells tend to swim side by side at first, then move away from each other with an acute angle, as shown in Fig. 8C,D. The final angle in this case seems to be independent of the initial angle, which will be discussed in detail below.

All the interacting cells were classified as HI, AR or ER, and the results are shown in Table 1. The total number of interacting cells recorded in this study was 602 (the total number of cases was 301). It was found that 84.7% of cells interact hydrodynamically. The ratio of ER is slightly higher than that of AR.

Numerical results

Although we have assumed that the experimental data not satisfying the definition of AR nor ER are HI, there is no evidence that two cells do not actively change their swimming motions during the interaction. Thus, we also performed numerical simulations. The authors used a squirmer model for some previous studies (Ishikawa et al., 2006; Pedley and Ishikawa, 2004) (T. Ishikawa and T. J. Pedley, manuscript submitted for publication), so a comparison with the earlier data was also made to check the reliability of the squirmer model.

We first show the interactions between two squirmers with $\theta_{in} \approx 0$ with a small distance between the squirmers in the perpendicular direction to the orientation vectors, as shown in Fig. 9. The orientation vectors of the squirmers are shown as large arrows on the ellipsoids, and a thin solid line is added so that one can easily compare the angle between the two squirmers. It is found from the figure that the two squirmers come very close to each other, then change their orientation in the near field, and finally move away from each other. This tendency is similar to the experimental results shown in Fig. 8A.

Fig. 10 shows the interactions between two squirmers with $\theta_{in} \approx 2\pi/3$, in which one squirmer collides with the posterior end of the other. We see that the two cells do not significantly change their swimming direction. This tendency is the same as the experimental results shown in Fig. 8B. If one squirmer collides with the anterior end of the other, on the other hand, the two cells tend to swim side by side at first, then move away from each other with an acute angle, as shown in Fig. 11. This tendency is again the same as the experimental results shown in Fig. 8C,D.

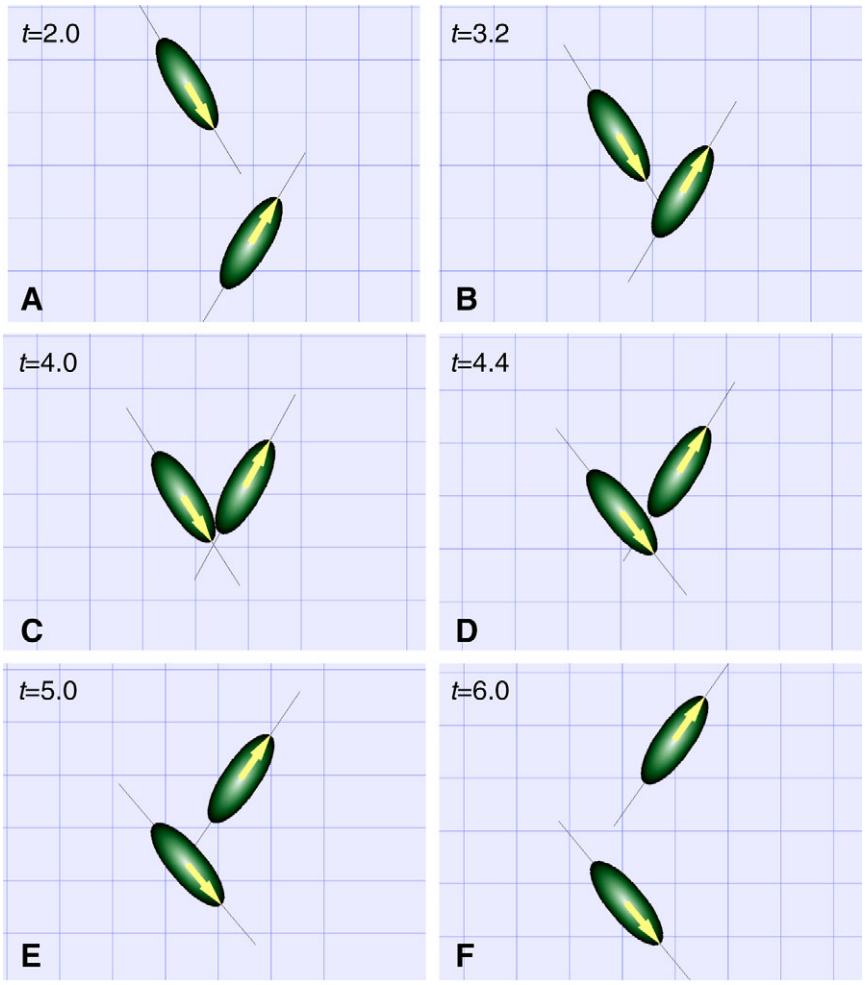

Fig. 10. Sequences (A–F) showing the hydrodynamic interactions between two squirmers under the initial condition of $\theta_{in} \approx 2\pi/3$. The orientation vectors of the squirmers are shown as large arrows on the ellipsoids, and a thin solid line is added so that one can easily compare the angle between the two squirmers. $d\theta$, explained in Fig. 12, is about 0.3 in this case. (A) t=2.0; (B) t=3.2; (C) t=4.0; (D) t=4.4; (E) t=5.0; (F) t=6.0.

Discussion

We can conclude from Table 1 that the cell–cell interaction is mainly hydrodynamic and that the biological reaction accounts for a minority of incidents. In the present experiment, the motion of cells was restricted between flat plates. In a real cell suspension, however, cells often swim freely in three-dimensional space. Since the effect of the walls on the cell behaviour is unclear, we performed a trial experiment in which cells swim three-dimensionally in a large container. In the trial experiment, we observed fewer biological reactions, because cells could avoid each other using three dimensions, and strong collisions occurred infrequently. We expect, therefore, that the

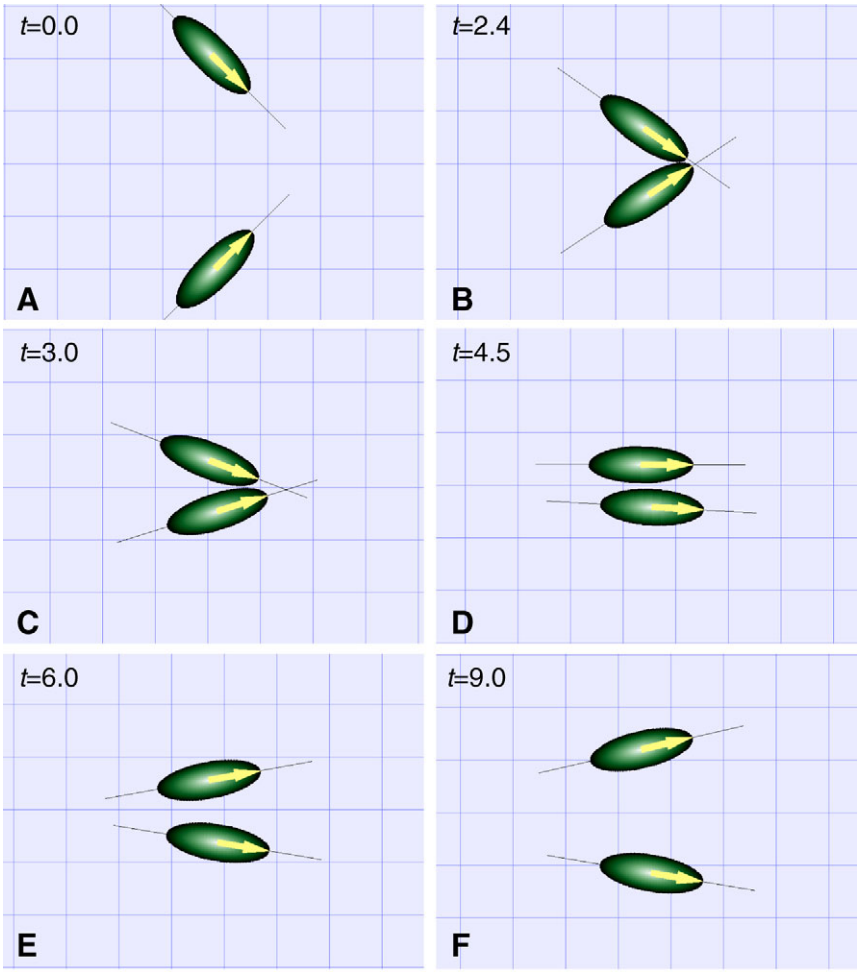

Fig. 11. Sequences (A–F) showing the hydrodynamic interactions between two squirmers under the initial condition of $\theta_{in} \approx \pi/2$. The orientation vectors of the squirmers are shown as large arrows on the ellipsoids, and a thin solid line is added so that one can easily compare the angle between the two squirmers. $d\theta$, explained in Fig. 12, is about 2.0 in this case. (A) t=0.0; (B) t=2.4; (C) t=3.0; (D) t=4.5; (E) t=6.0; (F) t=9.0.

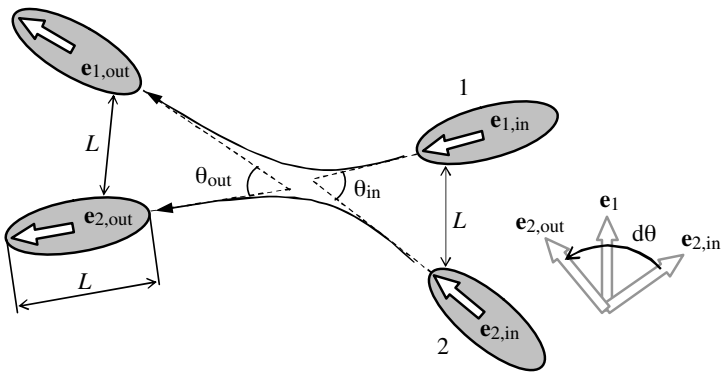

Fig. 12. Definition of three kinds of angles, where $\mathbf{e}_1$ and $\mathbf{e}_2$ are the orientation vectors of cell 1 and 2, respectively. θ_{in} is the angle between $\mathbf{e}_{1,in}$ and $\mathbf{e}_{2,in}$ when two cells surfaces are at a distance of L before the collision. θ_{out} is the angle between $\mathbf{e}_{1,out}$ and $\mathbf{e}_{2,out}$ when two cell surfaces are at a distance of L after the collision. In order to describes the change of orientation of cell 2 relative to cell 1, a frame is fixed to cell 1 so that the frame rotates when cell 1 rotates, and $d\theta$ is defined as change in the angle of cell 2 relative to this *rotating* frame.

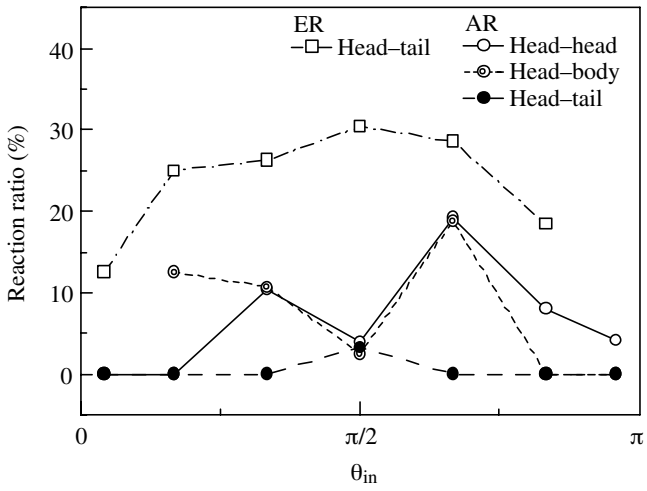

Fig. 13. Change of the reaction rate with θ_{in}. AR, avoiding reaction; ER, escape reaction. The data are classified according to the contact points. Head–tail, for instance, indicates that the collision occurs between the head of cell 1 and the tail of cell 2 (cf. Fig. 14).

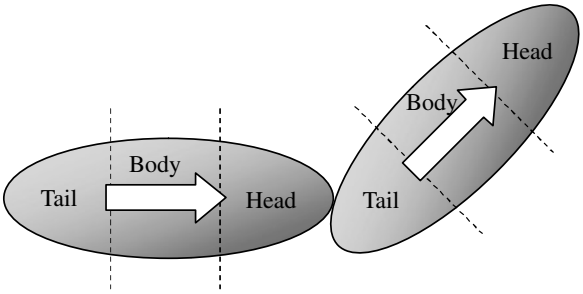

Fig. 14. Head–tail interaction, in which the collision occurs between the head of one cell and the tail of the other. A cell is divided into three equal length sections; head, body and tail, respectively, from the anterior end.

conclusion obtained here is also valid for cell–cell interactions in a cell suspension.

In order to analyse the experimental results quantitatively, we defined three angles during cell–cell interactions (see Fig. 12). θ_{in} is the angle between $\mathbf{e}_{1,in}$ and $\mathbf{e}_{2,in}$, where $\mathbf{e}_{i,in}$ is the orientation vector of cell i when the two cell surfaces are at a distance of L before the collision. θ_{out} is the angle between $\mathbf{e}_{1,out}$ and $\mathbf{e}_{2,out}$, where $\mathbf{e}_{i,out}$ is the orientation vector of cell i when the two cell surfaces are at a distance of L after the collision. In order to describe the change in orientation of cell 2 relative to cell 1, a frame is fixed to cell 1 so that the frame rotates when cell 1 rotates, and $d\theta$ is defined as the change in the angle of cell 2 relative to this rotating frame. Data for AR and ER are classified into seven θ_{in} ranges as well as three contact positions, where a cell is divided into three equal-length sections; head, body and tail, respectively from the anterior end. The reaction rates for each θ_{in} range and each contact position are shown in Fig. 13, where reaction rates are calculated by dividing the number of AR or ER for a certain θ_{in} range and a certain contact position by the total number of

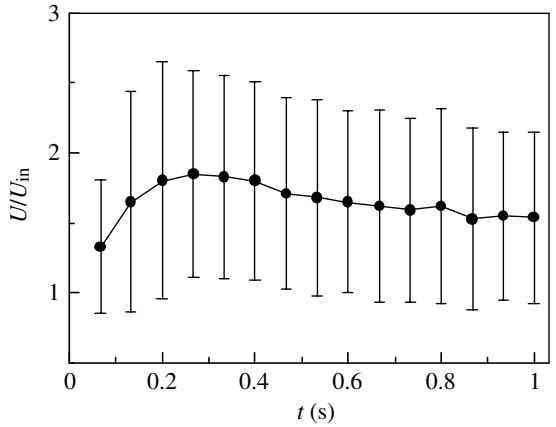

Fig. 15. Temporal change of swimming velocity in the case of escape reaction. Error bars show the standard deviation of 63 escaping cells. Collision occurs at t=0, and U_{in} is the velocity when two cell surfaces are at a distance of L before the collision.

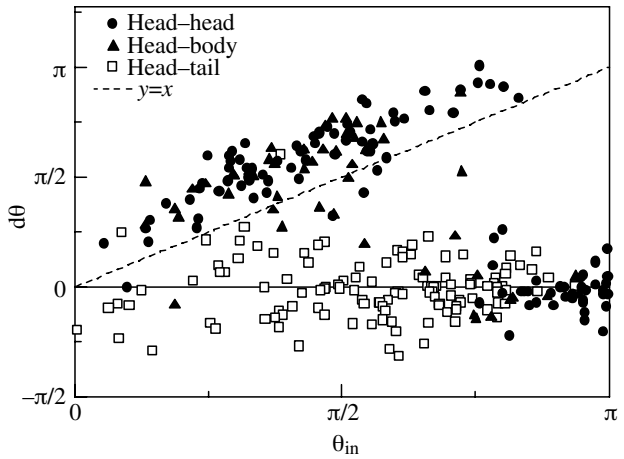

Fig. 16. Correlation between θ_{in} and $d\theta$ for the three contact positions. The broken line of slope one and the solid line of $d\theta$=0 are added for comparison.

cells under the same conditions. In Fig. 13, head–tail, for instance, indicates that the collision occurs between the head of one cell and the tail of the other (see Fig. 14). We see that AR occurs mostly when $\theta_{in}2\pi/3$ and under head–head or head–body conditions. AR rarely occurs under a head–tail condition. This is apparently because there are many Ca^{2+} channels in the anterior end, as explained in the Introduction.

ER occurs only when one cell collides with the tail of the other, and the reaction rate is not sensitive to θ_{in}, as shown in Fig. 13. The dependence of contact position can be explained by the locality of K^+ channels, as explained in the Introduction. The reaction rate of ER is higher than that of AR, so we can say that ER occurs more frequently in the cell–cell interaction. The temporal change of the dimension-free swimming velocity under

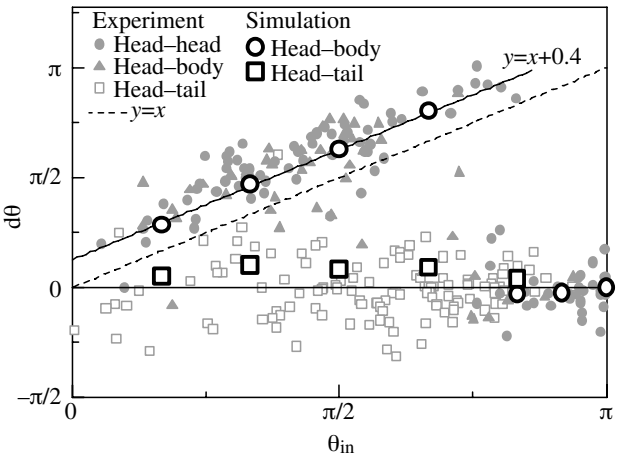

Fig. 17. Comparison of the results of $d\theta$ between the experiments and the simulations. Gray symbols, experimental results; the numerical results are plotted by large circles and squares. The broken line of slope one and the solid lines of $d\theta$=0 and $d\theta=\theta_{in}+0.4$ are added for comparison.

ER was measured, and the results are shown in Fig. 15. Since the escaping velocity depends on how strongly the posterior end of the cell is agitated, the error bar becomes very long. We see from the figure that the escaping velocity is maximum at t=0.2–0.3 s, and its value is about 1.8 times the initial velocity.

When a cell–cell interaction does not satisfy the definition of AR or ER, it is classified as HI. The correlations between $d\theta$ and θ_{in} for HI for the three contact positions are shown in Fig. 16. We see that $d\theta$ for head–tail (white squares) is distributed near $d\theta$=0, which means that the two cells do not change their orientations significantly after collision (cf. Fig. 8B). The cases for head–head and head–body, however, show a different tendency. When θ_{in} is smaller than approximately $3\pi/4$, $d\theta$ increases almost linearly with θ_{in}. A broken line with slope one is drawn in Fig. 16 for comparison. We see that $d\theta$ is slightly larger than θ_{in}, which means that the two cells tend to swim side by side at first, then move away from each other with a small angle, as shown in Fig. 8C,D. When θ_{in} is larger than approximately $3\pi/4$, $d\theta$ is distributed near $d\theta$=0, which again means that the two cells do not change their orientations significantly (cf. Fig. 8A). Consequently a tendency of the hydrodynamic interaction between two cells clearly appears, and is dependent on θ_{in} and contact position.

In order to compare numerical and experimental results quantitatively, we performed simulations for various θ_{in} conditions and for two contact positions (head–head and head–tail). The correlations between $d\theta$ and θ_{in} obtained in the simulations are shown in Fig. 17. We see that $d\theta$ for head–tail (large white squares) is distributed near $d\theta$=0, which is the same tendency as in the experiments. In the case of head–head (large white circles), $d\theta$ increases almost linearly with θ_{in} when θ_{in} is smaller than approximately $3\pi/4$. This tendency is also the same as in the experiments. The final angle θ_{out} for these squirmers is about 0.4 rad; thus, the numerical results fit well with $y=x+0.4$, as shown in the figure. When θ_{in} is larger than approximately $3\pi/4$, $d\theta$ is distributed near $d\theta$=0, which is again the same as in the experiments. We can conclude, therefore, that the HI data in the experiments agree well with the numerical results and that the interaction is purely hydrodynamic. Moreover, we can say that a squirmer model is appropriate for expressing the motion of *Paramecia*, and hopefully for some other ciliates as well.

In most of the previous analytical studies on cell–cell interactions (Guell et al., 1988; Ramia et al., 1993; Nasseri and Phan-Thien, 1997; Jiang et al., 2002), two cells in close contact were not discussed. [Lega and Passot (Lega and Passot, 2003) included an *ad hoc* interactive force acting between cells, which in practice is unlikely to exist.] The present results show, however, that the near-field interaction dramatically changes the orientation of cells. Since orientation change affects the macroscopic properties of the suspension, such as the diffusivity, the near-field interaction has to be solved accurately. The present results also show that the near-field interaction can be accurately solved hydrodynamically by the boundary element method and lubrication theory.

List of symbols

A_m	surface area of squirmer m
AR	avoiding reaction
$\mathbf{e}$	orientation vector of cell
ER	escape reaction
$\mathbf{F_{rep}}$	non-hydrodynamic interparticle repulsive force
$\mathbf{h}$	separation vector
HI	hydrodynamic interaction
$\mathbf{K}$	Oseen tensor
L	length
$\mathbf{q}$	single-layer potential (traction force on the inner surface minus that on the outer surface)
$\mathbf{U_m}$	translational velocity of squirmer m
$\mathbf{u_s}$	tangential surface velocity
$\mathbf{u_{s,m}}$	squirming velocity of squirmer m
$\mathbf{x_m}$	centre of squirmer m
$\mathbf{\Omega_m}$	rotational velocity of squirmer m
α_1, α_2	dimensionless coefficients
ϵ	minimum separation between two surfaces
θ	angle from the orientation vector of the cell

Appendix A

Velocity disturbance due to a force-free particle near a wall boundary

In Appendix A, we show that the velocity disturbance due to a force-free particle decays as r^{-2}, even though a no-slip wall boundary exists near the particle.

For an unbounded fluid, the Oseen tensor in Eqn 2 is given as:

$$K_{ij} = \frac{1}{8\pi\mu}\left(\frac{\delta_{ij}}{r} + \frac{r_i r_j}{r^3}\right), \quad \text{(A1)}$$

where μ is the viscosity, $\mathbf{r}=\mathbf{x}-\mathbf{x}'$, x is the position vector of the field point, and $\mathbf{x}'$ is the point where the traction force is generated.

In order to account for a no-slip wall boundary, we exploit an image system for the Oseen tensor. The image system was derived by Blake (Blake, 1971b), and a general outline of the method is included in standard texts (e.g. Kim and Karrila, 1992). If there is a wall boundary, the Oseen tensor needs to be rewritten as:

$$K'_{ij} = \frac{1}{8\pi\mu}\left[\left(\frac{\delta_{ij}}{r} + \frac{r_i r_j}{r^3}\right) - \left(\frac{\delta_{ij}}{R} + \frac{R_i R_j}{R^3}\right) + \frac{2b}{R^3}(\delta_{j3}R_i + \delta_{i3}R_j - 2\delta_{i3}\delta_{j3}R_3) + \frac{2b^2}{R^3}\left(2\delta_{i3}\delta_{j3} - \delta_{ij} + 3\frac{R_i}{R^2}(R_j - 2\delta_{j3}R_3)\right)\right], \quad \text{(A2)}$$

where $\mathbf{R}=\mathbf{x}-\mathbf{X}$, and $\mathbf{X}$ is the position vector of the image point that is the mirror image of $\mathbf{x}'$ about the wall boundary. The direction of subscript 3 is taken normal to the wall, and b is the minimum distance of $\mathbf{x}'$ or $\mathbf{X}$ from the wall (for details, see fig. 1 in Blake, 1971b). Eqn A2 indicates that the effect of the

wall boundary is equivalent to inducing a point force, a dipole and a source doublet at the image point.

When there are N particles and a wall boundary, the Stokes flow field around the particles can be given in an integral form as (similar to Eqn 2):

$$\mathbf{u}(\mathbf{x}) = -\sum_{m=1}^{N} \int_{A'_m} \mathbf{K}' \,.\, \mathbf{q}(\mathbf{x}')\mathrm{d}A'_m \,. \tag{A3}$$

The right-hand side of Eqn A3 can be expanded in moments about the centre of each particle and each image particle (see Durlofsky et al., 1987):

$$u_i(x) - \langle u_i(x)\rangle = \frac{1}{8\pi\mu}\sum_{\alpha=1}^{N}\left[\left(1+\frac{a^2}{6}\nabla^2\right)K_{ij}F_j^{\alpha} + \epsilon_{lkj}\tfrac{1}{4}(\nabla_k K_{il} - \nabla_l K_{ik})L_j^{\alpha} + \left(1+\frac{a^2}{10}\nabla^2\right)\tfrac{1}{2}(\nabla_k K_{ij} + \nabla_j K_{ik})S_{jk}^{\alpha} + \ldots\right] + \frac{1}{8\pi\mu}\sum_{\beta=1}^{N}\left[\left(1+\frac{a^2}{6}\nabla^2\right)\hat{K}_{ij}F_j^{\beta} + \epsilon_{lkj}\tfrac{1}{4}(\nabla_k \hat{K}_{il} - \nabla_l \hat{K}_{ik})L_j^{\beta} + \left(1+\frac{a^2}{10}\nabla^2\right)\tfrac{1}{2}(\nabla_k \hat{K}_{ij} + \nabla_j \hat{K}_{ik})S_{jk}^{\beta} + \ldots\right], \tag{A4}$$

where $\hat{\mathbf{K}}=\mathbf{K}'-\mathbf{K}$, and $\mathbf{F}$, $\mathbf{L}$ and $\mathbf{S}$ are, respectively, the monopole, the anti-symmetric dipole, and the symmetric dipole. Subscript α indicates real particles, and β indicates image particles. In the case of a force-free particle, $\mathbf{F}^{\alpha}=\mathbf{F}^{\beta}=0$. Hence, the leading-order term in the right-hand side of Eqn A4 is r^{-2} or R^{-2}. Therefore, the velocity disturbance due to a force-free particle decays as r^{-2}, even though a no-slip wall boundary exists near the particle.

Appendix B

A boundary condition of constant swimming power

In Appendix B, we show that the difference between two boundary conditions, constant surface velocity and constant swimming power, in the trajectories of two cells is small. A similar discussion has been published (Ishikawa et al., 2006).

Throughout this paper, the surface squirming velocity was assumed not to change during the interactions. Real micro-organisms, however, may well change their swimming motion in the presence of a nearby micro-organism. Of course, we did not model a cell's biological response to other micro-organisms, but we can apply a different primitive boundary condition for the squirmers to see if the effect is significant. In this boundary condition, the surface squirming velocity is defined as $\lambda\mathbf{u}_s$. Here, $\mathbf{u}_s$ is the squirming velocity for a solitary squirmer and λ is a scalar factor that is chosen to realize constant swimming power, equal to the rate of viscous energy dissipation throughout an interaction. The swimming power consumed by a squirmer is defined as:

$$\int_A \boldsymbol{\tau} \,.\, \mathbf{u}_s \mathrm{d}A \,, \tag{B1}$$

where $\boldsymbol{\tau}$ is the traction force on the surface.

We checked the relative translational–rotational velocities under the constant-swimming-power condition. However, the effect of changing the boundary condition was very small. This can be explained as follows. The surface velocity is proportional to λ, and the lubrication force is proportional to $\log(\epsilon^{-1})$ and λ, where ϵ is the gap distance between two surfaces [for a detailed discussion about the lubrication force, see Ishikawa et al. (Ishikawa et al., 2006)]. The power is the product of these two quantities in the near-field, thus proportional to $\log(\epsilon^{-1})$ and λ^2. In order to maintain constant power, λ should therefore vary as:

$$\lambda \propto \sqrt{\frac{1}{\log(\epsilon^{-1})}} \,. \tag{B2}$$

Because $\log(\epsilon^{-1})$ is a very weak singularity, λ changes very slowly. Thus, the difference between the two boundary conditions in the trajectories of two cells is small.

There may be some other boundary conditions for a swimming cell. Short et al., for instance, assumed constant surface stress instead of constant surface velocity (Short et al., 2006). However, the effect of this boundary condition should also be small, because the lubrication force between two cells is again not sufficiently strong, even if ϵ becomes the length scale of molecules, as mentioned above.

Appendix C

Effect of a wall boundary on the swimming velocity of a squirmer

In Appendix C, we show that the effect of a wall boundary on the translational velocity of a squirmer parallel to the wall is small if the distance between the two surfaces ϵ is larger than 10^{-4} or 10^{-5}.

We derived the first-order solution for the lubrication flow between a spherical squirmer and a sphere with arbitrary radius, in which a flat plate corresponds to infinitely large radius (Ishikawa et al., 2006). Although the squirmer model used in this study is spheroidal, we exploit the lubrication theory for a spherical squirmer in the following discussion for simplicity. The lubrication force due to the translational motion parallel to the wall is proportional to $\delta u \log(\epsilon^{-1})$ to the leading order, where δu is the velocity difference between the two surfaces in the lubrication region (cf. Ishikawa et al., 2006). δu can be rewritten as $\delta u = U + u_s|_{lub}$, where U is the translational velocity of the squirmer parallel to the wall and $u_s|_{lub}$ is the squirming velocity in the lubrication region. When the squirmer touches the wall, i.e. $\epsilon \to 0$, $\delta u \log(\epsilon^{-1})$ diverges to infinity unless $\delta u = 0$; thus, the squirmer swims with a

velocity of $-u_s|_{lub}$. When the surface squirming velocity is given by Eqn 1 and the orientation vector of the squirmer is parallel to the wall, the swimming velocity of the squirmer attached to the wall is about 1.5. Therefore, the wall boundary increases the swimming velocity of the squirmer by up to 50% when ϵ=0.

Next, we show how δu decays with ϵ. The lubrication force is generated by the relative motion between two surfaces in the lubrication region. This force has to be canceled by the viscous drag force acting outside the lubrication region, because the particle is force-free. Since the viscous drag force is not sensitive to ϵ, we can assume that the lubrication force is also unaffected by ϵ to the leading order, i.e. $\delta u \log(\epsilon^{-1})$=constant. Thus, δu decays as $1/\log(\epsilon^{-1})$. As mentioned in Appendix B, $\log(\epsilon^{-1})$ is a very weak singularity [$-\log(10^{-4})$=9.2 and $-\log(10^{-5})$=11.5, for instance]. We can conclude that the effect of a wall boundary on the translational velocity of a squirmer parallel to the wall is small if the distance between the two surfaces ϵ is larger than 10^{-4} or 10^{-5}. In the present experiment, ϵ is about 0.4, which is much larger than 10^{-4}.

The authors are grateful for helpful discussions with Prof. T. J. Pedley of DAMTP, University of Cambridge. The authors also appreciate Prof. Akitoshi Itoh of Tokyo Denki University for his kind help in dealing with the micro-organisms.

References

Bees, M. A. and Hill, N. A. (1998). Linear bioconvection in a suspension of randomly-swimming, gyrotactic micro-organisms. *Phys. Fluids* **10**, 1864-1881.

Blake, J. R. (1971a). A spherical envelope approach to ciliary propulsion. *J. Fluid Mech.* **46**, 199-208.

Blake, J. R. (1971b). A note on the image system for a stokeslet in a no-slip boundary. *Proc. Camb. Philos. Soc.* **70**, 303-310.

Brady, J. F. and Bossis, G. (1985). The rheology of concentrated suspensions of spheres in simple shear flow by numerical simulation. *J. Fluid Mech.* **155**, 105-129.

Brennen, C. and Winet, H. (1977). Fluid mechanics of propulsion by cilia and flagella. *Annu. Rev. Fluid Mech.* **9**, 339-398.

Childress, S., Levandowsky, M. and Spiegel, E. A. (1975). Pattern formation in a suspension of swimming micro-organisms: equations and stability theory. *J. Fluid Mech.* **63**, 591-613.

Claeys, I. L. and Brady, J. F. (1993). Suspensions of prolate spheroids in Stokes flow. Part 1. Dynamics of a finite number of particles in an unbounded fluid. *J. Fluid Mech.* **251**, 411-442.

Durlofsky, L., Brady, J. F. and Bossis, G. (1987). Dynamic simulation of hydrodynamically interacting particles. *J. Fluid Mech.* **180**, 21-49.

Fasham, M. J. R., Ducklow, H. W. and McKelvie, S. M. (1990). A nitrogen-based model of plankton dynamics in the oceanic mixed layer. *J. Mar. Res.* **48**, 591-639.

Grue, J., Jensen, A., Rusas, P.-O. and Sveen, J. K. (1999). Properties of large amplitude internal waves. *J. Fluid Mech.* **380**, 257-278.

Guell, D. C., Brenner, H., Frankel, R. B. and Hartman, H. (1988). Hydrodynamic forces and band formation in swimming magnetotactic bacteria. *J. Theor. Biol.* **135**, 525-542.

Hillesdon, A. J., Pedley, T. J. and Kessler, J. O. (1995). The development of concentration gradients in a suspension of chemotactic bacteria. *Bull. Math. Biol.* **57**, 299-344.

Ishikawa, T., Simmonds, M. P. and Pedley, T. J. (2006). Hydrodynamic interaction of two swimming model micro-organisms. *J. Fluid Mech.* **568**, 119-160.

Jiang, H., Osborn, T. R. and Meneveau, C. (2002). Hydrodynamic interaction between two copepods: a numerical study. *J. Plankton Res.* **24**, 235-253.

Keane, R. D. and Adrian, R. J. (1992). Theory of cross-correlation analysis of PIV images. *Appl. Sci. Res.* **49**, 191-215.

Kim, S. and Karrila, S. J. (1992). *Microhydrodynamics: Principles and Selected Applications.* Boston: Butterworth Heinemann.

Lega, J. and Passot, T. (2003). Hydrodynamics of bacterial colonies. *Phys. Rev. E* **67**, 1906.

Lighthill, M. J. (1952). On the squirming motion of nearly spherical deformable bodies through liquids at very small Reynolds numbers. *Commun. Pure Appl. Math.* **5**, 109-118.

Machemer, H. (1974). Frequency and directional responses of cilia to membrane potential changes in Paramecium. *J. Comp. Physiol.* **92**, 293-316.

Metcalfe, A. M. and Pedley, T. J. (2001). Falling plumes in bacterial bioconvection. *J. Fluid Mech.* **445**, 121-149.

Metcalfe, A. M., Pedley, T. J. and Thingstad, T. F. (2004). Incorporating turbulence into a plankton foodweb model. *J. Mar. Syst.* **49**, 105-122.

Naitoh, Y. and Sugino, K. (1984). Ciliary movement and its control in Paramecium. *J. Protozool.* **31**, 31-40.

Nasseri, S. and Phan-Thien, N. (1997). Hydrodynamic interaction between two nearby swimming micromachines. *Comp. Mech.* **20**, 551-559.

Pedley, T. J. and Ishikawa, T. (2004). Diffusion of swimming model micro-organisms in a semi-dilute suspension. *Bull. Am. Phys. Soc.* **49**, 142.

Pedley, T. J. and Kessler, J. O. (1990). A new continuum model for suspensions of gyrotactic micro-organisms. *J. Fluid Mech.* **212**, 155-182.

Pedley, T. J. and Kessler, J. O. (1992). Hydrodynamic phenomena in suspensions of swimming microorganisms. *Annu. Rev. Fluid Mech.* **24**, 313-358.

Ramia, M., Tullock, D. L. and Phan-Thien, N. (1993). The role of hydrodynamic interaction in the locomotion of microorganisms. *Biophys. J.* **65**, 755-778.

Short, M. B., Solari, C. A., Ganguly, S., Powers, T. R., Kessler, J. O. and Goldstein, R. E. (2006). Flows driven by flagella of multicellular organisms enhance long-range molecular transport. *Proc. Natl. Acad. Sci. USA* **103**, 8315-8319.